J. Fluid Mech. (1984), *vol.* 140, *pp.* 281–301
Printed in Great Britain

Viscous–inviscid interactions on axisymmetric bodies of revolution in supersonic flow

By A. KLUWICK, P. GITTLER

Institut für Strömungslehre und Wärmeübertragung, Technische Universität Wien, Wiedner Hauptstrasse 7, A-1040 Vienna, Austria

AND R. J. BODONYI

Department of Mathematical Sciences, Indiana University – Purdue University at Indianapolis, 1125 East 38th Street, Indianapolis, Indiana 46223

(Received 25 July 1983)

Using the method of matched asymptotic expansions, the interaction between axisymmetric laminar boundary layers and inviscid supersonic external flows is investigated in the limit of large Reynolds numbers. The resulting triple-deck equations are solved numerically for two different cases of body shapes: a cylinder–cone configuration and a configuration consisting of two concentric cylinders which are connected by a smooth curve. Solutions to the linearized as well as the fully nonlinear equations are presented.

1. Introduction

The general problem of viscous–inviscid interacting flows is of great importance in the theory of viscous flows in general and aerodynamics in particular. Although the problem has been extensively studied over the years, it has been only within the last decade that a rational theory has been developed which explains the complex nature of the viscous flow in this interaction region. In the case of laminar boundary layers the 'triple-deck' theories developed by Stewartson & Williams (1969) for supersonic flows, and Stewartson (1969) and Messiter (1970) for incompressible flows, play an essential role in the elucidation of the details of the flowfield. Since its original formulation, this theory has been applied to numerous interaction problems, many of which have been summarized in the review articles by Stewartson (1974, 1980, 1981), Messiter (1978, 1983), Kluwick (1979) and Smith (1982). As a consequence the basic properties of planar interacting flows seem to be well understood at present, although quantitative results are still lacking for a number of interesting and important problems, including for example, mixed transonic flows, owing to the computational difficulties associated with such flows.

In contrast, our understanding of three-dimensional viscous–inviscid interactions is much less complete. To date only a limited number of studies are available for three-dimensional interactions, owing, in part, to the numerical difficulties associated with such studies. The asymptotic triple-deck theory for two-dimensional flows has been generalized by Smith, Sykes & Brighton (1977) to account for three-dimensional disturbance of a Blasius boundary layer by considering a three-dimensional hump on an otherwise-flat surface. However, owing to the complexity of the inviscid outer-flow solution they were only able to obtain solutions to the linearized version of the governing equations. To study nonlinear effects, Sykes (1980) had to adopt a simplified model for the response of the outer flow to the displacement effects caused

by the boundary layer which in essence was based on a solution relevant to internal flows derived by Smith (1976). Nonlinear solutions that take into account the correct coupling between the boundary layer and the inviscid outer flow have been carried out so far only for swept-wing configurations (Vatsa & Werle 1977; Gittler 1984).

A second class of problems in which three-dimensional effects are of importance concerns viscous–inviscid interactions on axisymmetric bodies of revolution. Three different physical situations can occur in the study of axisymmetric interactions depending on the relationship between the body radius and the characteristic boundary-layer thickness. The flow situation most closely resembling that of the two-dimensional interaction problem occurs when the body radius is much larger than the boundary-layer thickness. Specifically, it has been shown by Duck (1984) for incompressible flow that when the body radius is of order $Re^{-\frac{3}{8}}$, where Re is a characteristic Reynolds number of the flow, the lower and main decks of triple-deck theory are unchanged from their two-dimensional form while the upper deck is now governed by the axisymmetric potential equation. As will be discussed below, a similar situation occurs for supersonic external streams, except that in this case the upper deck is governed by the axisymmetric wave equation.

The other two physical problems of interest occur when the body radius is of the order of the boundary-layer thickness and when the body radius is much less than the boundary-layer thickness. In both of these cases the body has become slender enough that the curvature effects are no longer negligible in the main and lower decks, respectively. Some discussion of the former case is given by Duck (1984) for incompressible flow, while the corresponding problems for supersonic mainstreams are currently under study.

Specifically, in this paper we discuss the response of a laminar boundary layer on an axisymmetric body of revolution placed in a supersonic mainstream when the body radius is of the order $Re^{-\frac{3}{8}}$. In §2 the appropriate boundary-value problem is formulated, while §3 deals with the asymptotic structure of the solutions far upstream. Finally, §§4 and 5 are devoted to the numerical and analytical study of the flow over bodies of revolution of the cylinder–cone type and the flow over two concentric cylinders that are connected by a smooth surface.

During the preparation of this paper a related study by Huang & Inger (1983) has appeared. In their study, however, they considered only the linearized version of the triple-deck interaction region studied in the present work. More significant, perhaps, are their results for the pressure and skin-friction distributions, shown in figures 5 and 6 of their paper. According to these figures the pressure gradient appears to be discontinuous at the corner, a result that we find not to be correct in this study. In addition, the results for the pressure and skin friction have the wrong asymptotic behaviour downstream of the corner. As will be pointed out in §2, these discrepancies seem to be caused by a mathematical error in equation (15) of their study.

2. Problem formulation

In this study we are concerned with the response of an axisymmetric boundary layers which forms on a cylindrical body of radius $\tilde{a}$ in a uniform supersonic stream with velocity $\tilde{u}_\infty$ due to small distortions on the surface of the cylinder. Let $\tilde{L}$ denote the distance of the distortion from the front of the cylinder and $\tilde{\nu}_\infty$ the kinematic viscosity in the external stream. In what follows it will be assumed that the Reynolds number $Re = \tilde{u}_\infty \tilde{L}/\tilde{\nu}_\infty$ is sufficiently large that

$$\epsilon = Re^{-\frac{1}{8}} \tag{1}$$

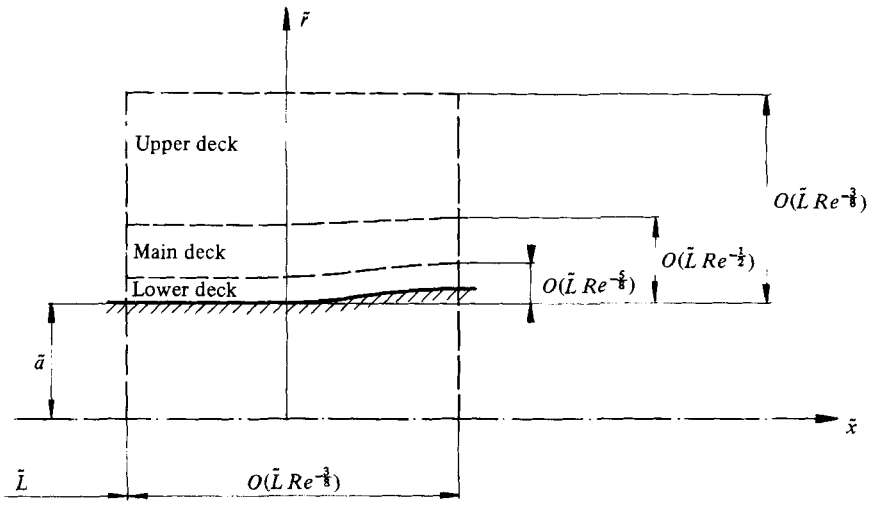

FIGURE 1. Triple-deck structure of the interaction region.

can be taken to be a small perturbation parameter. Furthermore, it will be assumed that

$$\bar{a} = \frac{\tilde{a}}{\epsilon^3 \tilde{L}} = O(1) \tag{2}$$

and that the deviations $\tilde{r}-\tilde{a}$ from the unperturbed cylindrical surface are of order

$$\tilde{r}/\tilde{a} = 1 + O(\epsilon^2). \tag{3}$$

Under these conditions the flow region affected by the viscous–inviscid interaction process develops a triple-deck structure in the limit $\epsilon \to 0$ considered here, as shown schematically in figure 1.

Owing to the scalings (2) and (3), both the boundary-layer thickness and the displacement of the boundary layer are sufficiently small that axisymmetric effects inside the undisturbed as well as the disturbed boundary layer are unimportant to leading order. Hence to a first approximation all axisymmetric effects are restricted to the flow outside of the boundary layer. Considering first this upper-deck region (see figure 1), we introduce the following non-dimensional variables:

$$\left.\begin{aligned} X &= \frac{\tilde{x}-\tilde{L}}{\epsilon^3 \tilde{L}}, \quad r = \frac{\tilde{r}}{\epsilon^3 \tilde{L}}, \quad p = \frac{\tilde{p}-\tilde{p}_\infty}{\tilde{\rho}_\infty \tilde{u}_\infty^2}, \\ u &= \frac{\tilde{u}}{\tilde{u}_\infty}, \quad v = \frac{\tilde{v}}{\tilde{u}_\infty}, \quad c = \frac{\tilde{c}}{\tilde{u}_\infty}, \end{aligned}\right\} \tag{4}$$

where $\tilde{x}$, $\tilde{r}$ denote the streamwise and radial coordinates, $\tilde{u}$, $\tilde{v}$ the corresponding velocity components, and $\tilde{c}$ the speed of sound. Furthermore it is assumed that the field quantities outside the boundary layer can be expanded in asymptotic series of the form

$$\left.\begin{aligned} u &= 1 + \epsilon^2 u_1(X,r) + \ldots, \quad v = \epsilon^2 v_1(X,r) + \ldots, \\ p &= \epsilon^2 p_1(X,r) + \ldots, \quad c = M_\infty^{-1} + \epsilon^2 c_1(X,r) + \ldots, \end{aligned}\right\} \tag{5}$$

where M_∞ denotes the Mach number of the undisturbed flow. Substituting (4) and (5) into the axisymmetric form of the Navier–Stokes equations yields to leading order the governing equations of the upper deck:

$$(1-M_\infty^2)\frac{\partial u_1}{\partial X} + \frac{\partial v_1}{\partial r} + \frac{v_1}{r} = 0, \quad \frac{\partial u_1}{\partial r} - \frac{\partial v_1}{\partial X} = 0. \tag{6}$$

Since the interaction process is induced by a distortion of the boundary of the cylinder, only outgoing waves are generated by the interaction. Hence the appropriate solutions to (6) can be expressed in the form

$$\left.\begin{aligned} u_1 &= -p_1 = -\frac{1}{4\pi}\int_0^\infty \bar{m}(X-\beta r\cosh\xi)\,\mathrm{d}\xi, \\ v_1 &= \frac{\beta}{4\pi}\int_0^\infty \bar{m}(X-\beta r\cosh\xi)\cosh\xi\,\mathrm{d}\xi, \end{aligned}\right\} \tag{7}$$

where $\beta = (M_\infty^2-1)^{\frac{1}{2}}$, and $\bar{m}(\xi)$ is related to the source-distribution function. Note that in contrast with slender-body theory the disturbances of u and v are of the same order of magnitude. As a consequence p_1 is directly related to u_1 as in planar flows, but does not contain terms proportional to v_1^2. In addition, it is possible to derive a relationship between the pressure disturbances and the normal velocity component at the surface of the unperturbed cylinder $r = \bar{a}$ (Lighthill 1945; Ward 1948). This result forms the basis of the investigation by Huang & Inger (1983). Unfortunately, however, they did not recognize the typographical error in equation (83.8) of Ward (1955), and thus state the Laplace transform of the function $W(s)$ that enters their formulation as $\overline{W} = (K_1-K_0)/K_1$.† Here K_0 and K_1 are the modified Bessel functions of 0th and 1st order, respectively. It is this error in Huang & Inger (1983) which introduces a singularity strong enough to destroy the convergence of the pressure at large distances and leads to their unphysical results.

As remarked earlier, assumptions (2) and (3) imply that the structure of the flow in the boundary layer is the same as in two-dimensional flows to leading order. Introducing the stretched distance y_m from the unperturbed surface of the cylinder,

$$y_\mathrm{m} = \frac{\tilde{r}-\tilde{a}}{\epsilon^4\tilde{L}}, \tag{8}$$

it is easily shown that the solution in the main deck $y_\mathrm{m} = O(1)$ is identical with that of the planar flow, viz

$$\left.\begin{aligned} u &= U_0(y_\mathrm{m})+\epsilon A_1(X)\,U_0'(y_\mathrm{m})+\ldots, \\ v &= -\epsilon^2 A_1'(X)\,U_0(y_\mathrm{m})+\ldots, \\ \rho &= R_0(y_\mathrm{m})+\epsilon A_1(X)\,R_0'(y_\mathrm{m})+\ldots, \\ p &= \epsilon^2 p_1(X)+\ldots, \end{aligned}\right\} \tag{9}$$

where U_0 and R_0 denote the axial velocity and the density distributions in the unperturbed boundary layer.

Finally, the expansions for the lower deck $y_1 = y_\mathrm{m}/\epsilon = O(1)$ are

$$\left.\begin{aligned} u &= \lambda y_1+\epsilon u_1^1(X,y_1)+\ldots, \\ v &= \epsilon^3 v_1^1(X,y_1)+\ldots, \\ p &= \epsilon^2 p_1(X)+\ldots, \\ \rho &= R_0(0)+\epsilon\rho_1^1(X,y_1)+\ldots, \end{aligned}\right\} \tag{10}$$

where $\lambda = 0.332$ just as in the planar case, which follows immediately from (1) and the Seban–Bond–Kelly approximation (e.g. Stewartson 1955).

For simplicity in the numerical computations it is convenient to scale as many of

† The authors are indebted to one of the referees for pointing out this error in the paper by Huang & Inger.

the physical parameters as possible out of the problem. To this end consider the following transformation of variables:

$$\left.\begin{aligned} X &= C^{\frac{3}{8}}\lambda^{-\frac{5}{4}}|M_\infty^2-1|^{-\frac{3}{8}}(T_w/T_\infty)^{\frac{3}{2}}x,\\ y_1 &= C^{\frac{5}{8}}\lambda^{-\frac{3}{4}}|M_\infty^2-1|^{-\frac{1}{8}}(T_w/T_\infty)^{\frac{3}{2}}y,\\ p_1 &= C^{\frac{1}{4}}\lambda^{\frac{1}{2}}|M_\infty^2-1|^{-\frac{1}{4}}p,\\ u_1^1 &= C^{\frac{1}{8}}\lambda^{\frac{1}{4}}|M_\infty^2-1|^{-\frac{1}{8}}(T_w/T_\infty)^{\frac{1}{2}}u,\\ v_1^1 &= C^{\frac{3}{8}}\lambda^{\frac{3}{4}}|M_\infty^2-1|^{\frac{1}{8}}(T_w/T_\infty)^{\frac{1}{2}}v,\\ A_1 &= C^{\frac{5}{8}}\lambda^{-\frac{3}{4}}|M_\infty^2-1|^{-\frac{1}{8}}(T_w/T_\infty)^{\frac{3}{2}}A,\\ \bar{a} &= c^{\frac{3}{8}}\lambda^{-\frac{5}{4}}|M_\infty^2-1|^{-\frac{7}{8}}(T_w/T_\infty)^{\frac{3}{2}}a,\\ \bar{m} &= C^{\frac{1}{4}}\lambda^{\frac{1}{2}}|M_\infty^2-1|^{-\frac{1}{4}}m, \end{aligned}\right\} \tag{11}$$

where C is the Chapman constant occurring in the linear viscosity law

$$\tilde{\mu}/\tilde{\mu}_\infty = C(\tilde{T}/\tilde{T}_\infty),$$

and T_w denotes the non-dimensional wall temperature. Hence the governing equations in the lower deck, to leading order, reduce to

$$u\frac{\partial u}{\partial x}+v\frac{\partial u}{\partial y} = -\frac{\mathrm{d}p}{\mathrm{d}x}+\frac{\partial^2 u}{\partial y^2}, \quad \frac{\partial u}{\partial x}+\frac{\partial v}{\partial y}=0. \tag{12}$$

The no-slip conditions require that

$$u = v = 0 \quad \text{for} \quad y = F(x), \quad F(x)\to 0 \quad \text{as} \quad x\to-\infty, \tag{13}$$

while matching the solution through the main and upper decks, along with the condition that disturbances induced by the interaction vanish as $x\to-\infty$, yields the following conditions:

$$\left.\begin{aligned} &u = y+A(x), \quad y\to\infty, \quad \text{all } x,\\ &u = y, \quad x\to-\infty, \quad \text{all } y,\\ &p(x) = \frac{1}{4\pi}\int_0^\infty m(x-a\cosh\rho)\,\mathrm{d}\rho,\\ &A'(x) = -\frac{1}{4\pi}\int_0^\infty m(x-a\cosh\rho)\cosh\rho\,\mathrm{d}\rho. \end{aligned}\right\} \tag{14}$$

Finally, to simplify the numerical computations, (12)–(14) are transformed using Prandtl's transposition theorem (e.g. Rosenhead 1963). Introducing the variables

$$z = y-F(x), \quad w = v-uF'(x), \tag{15}$$

it is easily shown that the boundary-value problem reduces to

$$\left.\begin{aligned} &u\frac{\partial u}{\partial x}+w\frac{\partial u}{\partial z} = -\frac{\mathrm{d}p}{\mathrm{d}x}+\frac{\partial^2 u}{\partial z^2}, \quad \frac{\partial u}{\partial x}+\frac{\partial w}{\partial z}=0,\\ &u = w = 0 \quad \text{at} \quad z = 0,\\ &u\to z \quad \text{as} \quad x\to-\infty, \quad \text{all } z,\\ &u\to z+A(x)+F(x) \quad \text{as} \quad z\to\infty, \quad \text{all } x,\\ &p(x) = \frac{1}{4\pi}\int_0^\infty m(x-a\cosh\rho)\,\mathrm{d}p,\\ &A'(x) = -\frac{1}{4\pi}\int_0^\infty m(x-a\cosh\rho)\cosh\rho\,\mathrm{d}\rho. \end{aligned}\right\} \tag{16}$$

Before considering the solution of the boundary-value problem for several choices of $F(x)$ we first consider the asymptotic structure of the solution for $x\to-\infty$.

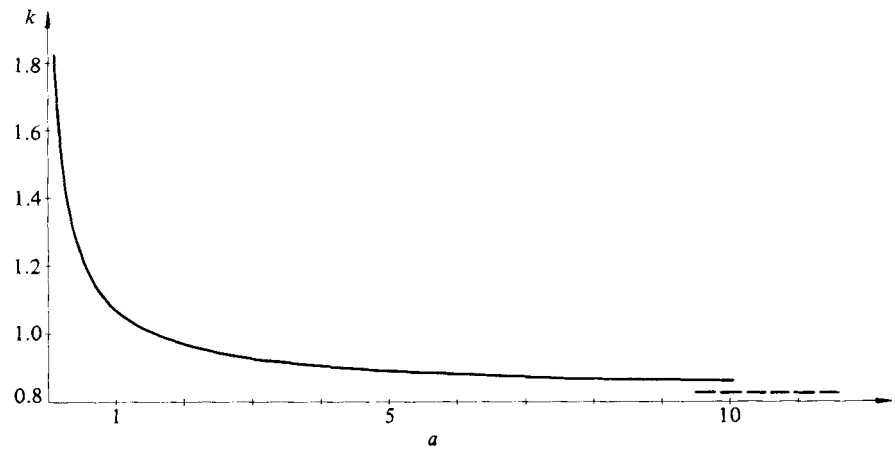

FIGURE 2. Dependence of the upstream decay rate k on the body radius a.

3. Asymptotic structure for $x \to -\infty$

The results derived by Lighthill (1953) and Stewartson & Williams (1969) for planar boundary layers suggest that the solutions to (12)–(14) for $x \to -\infty$ can be expressed in the form

$$\left.\begin{aligned} u &= y + \delta\, \mathrm{e}^{kx} f'(y) + O(\delta^2), \\ v &= -\delta k\, \mathrm{e}^{kx} f(y) + O(\delta^2), \\ m &= \delta\, \mathrm{e}^{kx} + O(\delta^2). \end{aligned}\right\} \tag{17}$$

Substituting (17) into (12)–(14), it is easily shown that

$$f'(y) = \frac{k^{\frac{1}{3}}}{4\pi\, \mathrm{Ai}'(0)} K_1(ka) \int_0^{k^{\frac{1}{3}} y} \mathrm{Ai}\,(s)\, \mathrm{d}s \tag{18}$$

and

$$\left.\begin{aligned} p(x) &\sim \frac{\delta}{4\pi} \mathrm{e}^{kx} K_1(ka), \\ A'(x) &\sim -\frac{\delta}{4\pi} \mathrm{e}^{kx} K_0(ka), \end{aligned}\right\} \tag{19}$$

where $\mathrm{Ai}\,(s)$ is the Airy function and K_0 and K_1 are the modified Bessel functions of 0th and 1st order respectively. It also follows that k satisfies the relationship

$$k^{\frac{4}{3}} = -3\, \mathrm{Ai}'\,(0) \frac{K_1(ka)}{K_0(ka)}. \tag{20}$$

In the limit $a \to \infty$ the expressions derived so far reduce to the appropriate two-dimensional results; i.e. since $K_1(ka) \to K_0(ka)$ as $ka \to \infty$, (3.20) gives

$$k^{\frac{4}{3}} = -3\, \mathrm{Ai}'\,(0). \tag{21}$$

Similarly, expansion of the dispersion relationship (20) for $ka \to 0$ yields

$$(ka)^{\frac{7}{3}} \ln (ka) \sim 3a^{\frac{4}{3}}\, \mathrm{Ai}'\,(0), \tag{22}$$

which indicates that $k \to \infty$ as $a \to 0$. The numerical solution of the dispersion relationship (20) is shown in figure 2, and the solution confirms the limiting behaviours for k as $a \to 0, \infty$. Since $k \to \infty$ as $a \to 0$, the upstream influence vanishes on

the lengthscale $\epsilon^3\tilde{L}$ used. Therefore, to resolve the structure of the interaction process in this limit, a different scaling of the interaction region must be considered where the body radius scales with the classical boundary-layer thickness as noted in §1.

4. Cylinder–cone configuration: linearized solution

In the following it will be assumed that the cylindrical surface of the body is composed of a right circular cylinder for $x \leqslant 0$ and a cone of small apex angle $\alpha^* = O(\epsilon^2)$ for $x > 0$. Thus

$$F(x) = \alpha x H(x), \quad \alpha = C^{-\frac{1}{4}}\lambda^{-\frac{1}{2}}(M_\infty^2 - 1)^{-\frac{1}{4}}\frac{\alpha^*}{\epsilon^2}, \tag{23}$$

where $H(x)$ is the Heaviside step function. On the assumption that α is sufficiently small, we can expand the field variables as power series in α in the following manner:

$$\left.\begin{aligned} u(x,z) &= z + \alpha u_1(x,z) + O(\alpha^2), \\ w(x,z) &= \alpha w_1(x,z) + O(\alpha^2), \\ p(x) &= \alpha p_1(x) + O(\alpha^2), \\ A(x) &= \alpha A_1(x) + O(\alpha^2), \\ m(x) &= \alpha m_1(x) + O(\alpha^2), \end{aligned}\right\} \tag{24}$$

where u_1, w_1, p_1, A_1 and m_1 satisfy the set of equations

$$\left.\begin{aligned} z\frac{\partial u_1}{\partial x} + w_1 = -\frac{\mathrm{d}p_1}{\mathrm{d}x} + \frac{\partial^2 u_1}{\partial z^2}, \quad \frac{\partial u_1}{\partial x} + \frac{\partial w_1}{\partial z} = 0, \\ u_1 = w_1 = 0 \quad \text{on} \quad z = 0 \quad \text{for all } x, \\ u_1 \to 0 \quad \text{as} \quad x \to -\infty \quad \text{for all } z, \\ u_1 \to xH(x) + A_1(x) \quad \text{as} \quad z \to \infty \quad \text{for all } x, \\ p_1(x) = \frac{1}{4\pi}\int_0^\infty m_1(x - a\cosh\rho)\,\mathrm{d}\rho, \\ A_1(x) = -\frac{1}{4\pi}\int_0^\infty m_1(x - a\cosh\rho)\cosh\rho\,\mathrm{d}\rho. \end{aligned}\right\} \tag{25}$$

To eliminate the source function $m_1(x)$ the momentum equation (25) is differentiated first with respect to z, which leads to a differential equation for the shear stress $\tau_1 = \partial u_1/\partial z$. Introducing the Fourier transform

$$\bar{\tau}(z;\omega) = \frac{1}{2\pi}\int_{-\infty}^{\infty} \tau_1(x,z)\,\mathrm{e}^{-\mathrm{i}\omega x}\,\mathrm{d}x \tag{26}$$

for τ as well as for all the other field variables, one obtains the following boundary-value problem:

$$\frac{\partial^2\bar{\tau}}{\partial z^2} - \mathrm{i}\omega z\bar{\tau} = 0, \tag{27}$$

$$\bar{\tau} = 0 \quad \text{for} \quad z \to \infty, \tag{28}$$

$$\bar{\tau}_z|_{z=0} = \omega^2\frac{K_0(\mathrm{i}\omega a)}{K_1(\mathrm{i}\omega a)}\left[\int_0^\infty \bar{\tau}\,\mathrm{d}z - \frac{\bar{F}}{\alpha}\right].$$

Once $\bar{\tau}$ has been determined from (27) and (28), $\bar{p}_1$ and $\bar{A}_1$ follow from

$$\left.\begin{aligned} \bar{p}_1 &= \frac{1}{\mathrm{i}\omega}\bar{\tau}_z|_{z=0}, \\ \bar{A}_1 &= \int_0^\infty \bar{\tau}\,\mathrm{d}z - \frac{\bar{F}}{\alpha}, \end{aligned}\right\} \tag{29}$$

where, for the linear-ramp problem,

$$\frac{\bar{F}}{\alpha} = \frac{1}{2\pi(\mathrm{i}\omega)^2}. \tag{30}$$

Evaluation of (27) and (28) for $a \to \infty$ and $a \to 0$ yields the following expressions

$$\left.\begin{aligned} \bar{p}_1 &\sim -\mathrm{i}\omega\bar{A}_1 \quad \text{as} \quad a \to \infty, \\ \bar{p}_1 &\sim -\omega^2 a \ln a \bar{A}_1 \quad \text{as} \quad a \to 0. \end{aligned}\right\} \tag{31}$$

Thus the result for plane supersonic flow

$$p = -A'$$

is recovered in the limit $a \to \infty$, while the relationship between A and p reduces to

$$p = -a \ln a A'', \tag{32}$$

for $a \to 0$ as in the case of incompressible flow studied by Duck (1984). The solution to (27) and (28) can be expressed in the form

$$\left.\begin{aligned} \bar{\tau}(z;\omega) &= \frac{3\,\mathrm{Ai}\,[(\mathrm{i}\omega)^{\frac{1}{3}} z]}{2\pi(\mathrm{i}\omega)^{\frac{1}{3}} g(\omega, a)}, \\ \bar{p}_1(\omega) &= \frac{3\,\mathrm{Ai}'(0)}{2\pi(\mathrm{i}\omega)\, g(\omega, a)}, \\ g(\omega, a) &= 3\mathrm{Ai}'(0)\frac{K_1(\mathrm{i}\omega a)}{K_0(\mathrm{i}\omega a)} + (\mathrm{i}\omega)^{\frac{4}{3}}. \end{aligned}\right\} \tag{33}$$

The inversion of the Fourier-integral transformation presents no difficulty when $x \leqslant 0$. A straightforward application of the residue theorem yields

$$\left.\begin{aligned} \tau_1(x, z) &= \frac{9\,\mathrm{Ai}\,(k^{\frac{1}{3}} z)}{4k^{\frac{2}{3}}} Q(k;a)\,\mathrm{e}^{kx}, \\ p_1(x) &= -\frac{9\,\mathrm{Ai}'(0)}{4k^{\frac{4}{3}}} Q(k;a)\,\mathrm{e}^{kx}, \\ Q(k;a) &= \frac{16 K_0(ka)\, k^{\frac{4}{3}} a}{16 K_0(ka)\, k^{\frac{4}{3}} - 9\,\mathrm{Ai}'(0)\, K_1(ka)}, \end{aligned}\right\} \tag{34}$$

where k is the solution of (20).

No simple analytical expression for the field variables could be found when $x > 0$. Therefore the inversion of the Fourier integral was carried out numerically by means of the fast-Fourier-transformation method of Cooley & Tukey (1965). Solutions were obtained for $a = 0.5$, 1, 5, 10 and ∞. $\tau(x, 0)$ and $p(x)$ were evaluated at 12288 grid points, and in all cases the computations were performed for various different mesh sizes Δx in order to obtain sufficient accuracy for small as well as large distances from the corner. Comparison of the numerical results and the analytical expression (34) at $x = 0$ showed that the differences were less than 1 % for $a = 1$, 5, 10 and ∞, and

less than 3% for $a = 0.5$. Furthermore, comparison of the wall-shear-stress and pressure distribution for $a = \infty$ and the analytical results for plane flow obtained by Stewartson (1970*a*, *b*, 1971) yielded agreement to 3 decimal places over the whole computational domain.

A further means to check the accuracy of the numerical data is provided by the asymptotic structure of the linearized solution as $x \to \infty$. Inspection of (33) shows that

$$\bar{p}_1 \sim -\frac{a}{2\pi} \ln (\mathrm{i}\omega) \tag{35}$$

for $\omega \to 0$, a fixed. Evaluation of the inverse Fourier integral (e.g. Lighthill 1958) then yields the asymptotic result

$$p \sim \frac{\alpha a}{x} \quad \text{as} \quad x \to \infty. \tag{36}$$

In marked contrast with the two-dimensional case, therefore, the pressure disturbance decays to zero as $x \to \infty$. This is a direct consequence of the increase of the streamtube area downstream of the corner caused by the axial symmetry of the flowfield. Using the properties of $\bar{\tau}_1(0, \omega)$ for the small values of ω,

$$\bar{\tau}_1(0, \omega) \sim -\frac{a}{2\pi} \frac{\mathrm{Ai}\,(0)}{\mathrm{Ai}'\,(0)} (\mathrm{i}\omega)^{\frac{2}{3}} \ln (\mathrm{i}\omega a) \quad \text{as} \quad \omega \to 0. \tag{37}$$

The behaviour of the wall-shear-stress distribution for $x \to \infty$ can also be evaluated. One obtains

$$\tau(x, 0) \sim 1 - \frac{2\alpha a\, \mathrm{Ai}\,(0)}{3\, \mathrm{Ai}'\,(0)\, \Gamma(\frac{1}{3})} \frac{1}{x^{\frac{5}{3}}} \left[\ln \frac{x}{a} - \psi(-\tfrac{5}{3}) \right] \quad \text{as} \quad x \to \infty. \tag{38}$$

Here $\psi(x)$ denotes the digamma function (e.g. Lighthill 1958).

Comparison between the numerical results and the asymptotic expressions (36) and (38) showed excellent agreement.

It should be noted that (36) can also be derived directly by evaluating (27)–(29) for $\omega \to 0$. Consequently, (36) and (38) also hold in the nonlinear case where $\alpha = O(1)$, which is considered in §5.

Figures 3 and 4 summarize the numerical solutions for $a = 0.5$, 1, 5, 10 and ∞. As in the case of two-dimensional flows, the slope of the wall-shear-stress distribution is discontinuous at $x = 0$, while the slope of the pressure distribution there is continuous. An analysis similar to that given by Brilliant & Adamson (1973) for two-dimensional transonic flow or direct evaluation of (33) for small a yields

$$\left.\begin{aligned} p(x) &\sim p(0-) + p'(0-)\, x + O(x^{\frac{4}{3}}), \\ \tau_{\mathrm{w}}(x) &\sim \tau_{\mathrm{w}}(0-) + O(x^{\frac{2}{3}}). \end{aligned}\right\} \tag{39}$$

As can be seen from figure 3, the exponential growth of the pressure disturbances upstream of the corner is followed by a much milder increase leading to a maximum value followed by a gradual decrease to its unperturbed level. With decreasing value of a the maximum disturbance induced by the interaction process decreases and the pressure decays more rapidly in agreement with the asymptotic result (34). While the pressure disturbance at $x = 0$ is independent of a according to purely inviscid theory, viscosity clearly leads to a marked reduction of the interaction pressure even for moderate values of a.

The properties of the pressure distribution have two immediate consequences for

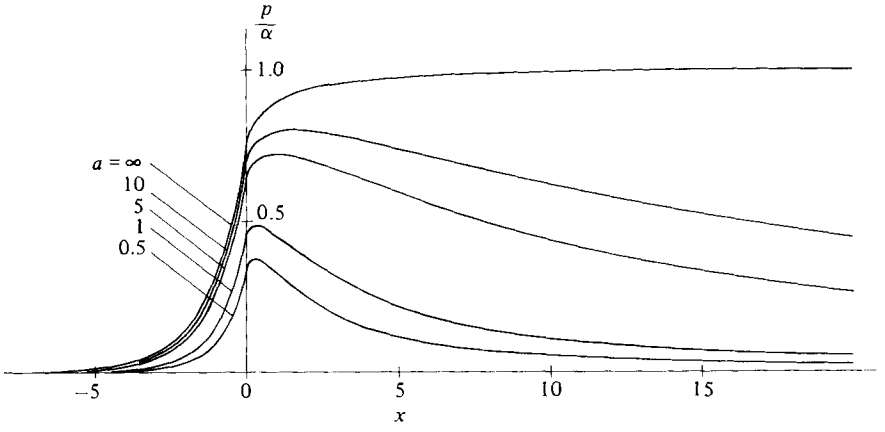

FIGURE 3. Cylinder–cone configuration: pressure distribution for various values of a according to linear theory.

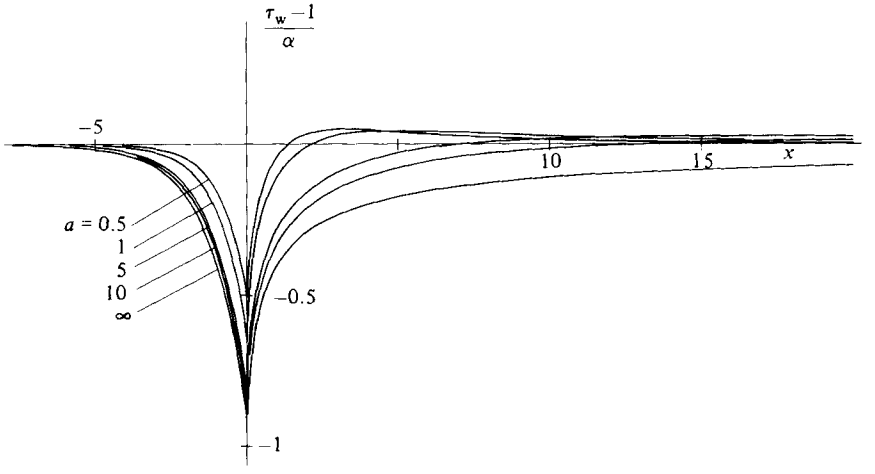

FIGURE 4. Cylinder–cone configuration: shear-stress distribution for various values of a according to linear theory.

the wall-shear-stress distribution (figure 4). Since the maximum pressure disturbance decreases with decreasing body radius a, the shear-stress perturbation also decreases with decreasing a. As was to be expected (and as will be verified in §5), this indicates that axisymmetric boundary layers can sustain larger positive turning angles than two-dimensional boundary layers before separation occurs. Furthermore, since the pressure gradient is favourable far downstream, the shear-stress disturbance is positive for sufficiently large values of x (equation 38), similar to that found in two-dimensional subsonic flows.

5. Cylinder–cone configuration: nonlinear results

In addition to the linear solutions discussed in §4, solutions to the full nonlinear interaction equations (16) have also been obtained. To this end the momentum equation is again differentiated with respect to z as in the linear case. Fourier

transformation of the resulting relationship and the boundary conditions then leads to

$$\left.\begin{aligned} \mathrm{i}\omega\bar{\tau}-\frac{\partial^2\bar{\tau}}{\partial z^2} &= -\overline{\left[u^*\frac{\partial\tau^*}{\partial x}+w\frac{\partial\tau^*}{\partial z}\right]}, \\ \bar{\tau} &= 0 \quad \text{for} \quad z\to\infty, \\ \bar{\tau}_z|_{z=0} &= \omega^2\frac{K_0(\mathrm{i}\omega a)}{K_1(\mathrm{i}\omega a)}\left[\int_0^\infty \bar{\tau}\,\mathrm{d}z-\bar{F}\right], \end{aligned}\right\} \tag{40}$$

where $u^* = u-z$, $\tau^* = \tau-1$, and $\bar{\tau}$ is the Fourier transform of τ^*.

Similar to the numerical investigation of two-dimensional interacting flows by Burggraf & Duck (1981), (40) and (29) were cast into finite-difference form using central differences. The resulting set of equations was then solved iteratively by evaluating the right-hand side of (40) from the results obtained from the previous iteration. Starting from the linear solution to (40), the iterations were carried out until the corrections $\Delta\tau$ were less than 10^{-5} in absolute value for all meshpoints x_i, z_i.

Solutions were again obtained for $a = 0.5$, 1, 5, 10 and ∞. In each case the number of meshpoints in the z-direction was 45 and the Fourier transform $\bar{\tau}(z;\omega)$ was calculated for 256 discrete values of ω equispaced over the interval $-128\Delta\omega \leqslant \omega \leqslant 127\Delta\omega$. Application of the fast-Fourier-transform method then yielded $\tau(z,x)$ inside the streamwise region $-128\Delta x \leqslant x \leqslant 127\Delta x$, where $\Delta x = \pi/(128\Delta\omega)$. Owing to the slow algebraic decay of τ as $x\to\infty$, a rather large streamwise extent of the computational domain was needed, even for moderate values of a. Extensive test runs showed that by taking $0.25 \leqslant \Delta x \leqslant 0.5$ numerical solutions are obtained which allow both for sufficient resolution near $x = 0$ and for the rather long streamwise extent necessary owing to the slow algebraic decay of the solution far downstream. Therefore the computational domain extended over $0 \leqslant y \leqslant 22$ and $-32(64) \leqslant x \leqslant 31.85(63.5)$.

Numerical computations based on the wall geometry (23) showed that strong oscillations occurred in the wall-shear-stress distribution already at moderately large values of the transformed ramp angle α. To eliminate these oscillations, which are caused by the discontinuous change of the boundary condition at $x = 0$, a smoothed version of the cylinder–cone problem characterized by

$$F = \alpha x H(x) \quad (|x| > \rho), \quad F = \alpha\left[\frac{x^2}{4\rho}+\frac{x}{2}+\frac{\rho}{4}\right] \quad (-\rho \leqslant x \leqslant \rho) \tag{41}$$

and

$$\bar{F} = \frac{1}{2\pi}\frac{\alpha}{(\mathrm{i}\omega)^2}\frac{\sin\omega\rho}{\omega\rho} \tag{42}$$

was considered. Numerical calculations carried out for $\rho = 1$ yielded smooth distributions of the field quantities over the entire streamwise extent of the computational domain for $\alpha > 0$ (compression corner) as well as $\alpha < 0$ (expansion corner).

The application of the spectral method outlined so far leads to distributions of the wall shear stress and the pressure which do not decay monotonically as x approaches the left end of the computational domain, but rather change sign and then start to increase again slightly as shown in figure 5 and also as observed by Burggraf & Duck (1981). For the case of axisymmetric flows considered here, this behaviour is a direct consequence of the asymptotic properties of the solution given by (17), (36)

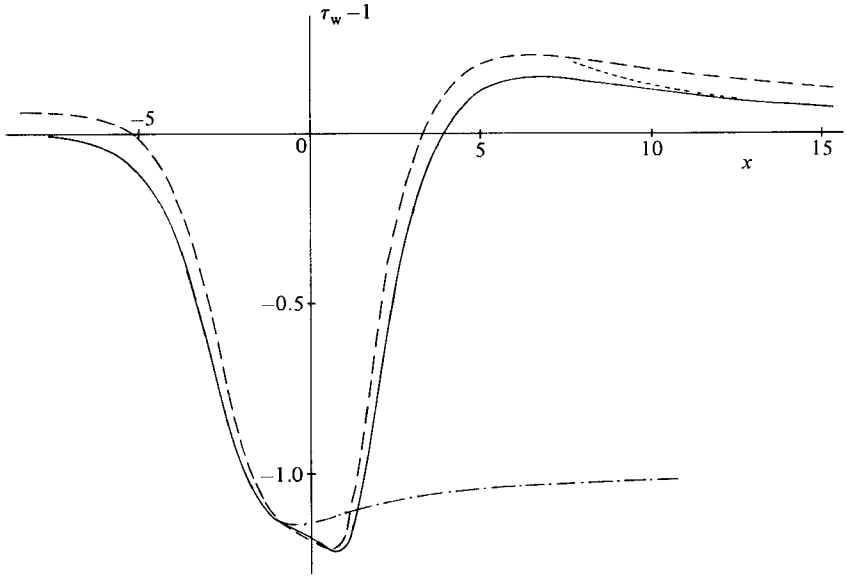

FIGURE 5. Cylinder–cone configuration given by (41): shear-stress distribution for $a = 1$ and $\alpha = 5$: ——, spectral method; ——, modified spectral method; –·–·–, free-interaction solution. --------, asymptotic relationship (38).

and (38), and the resulting error is therefore inherent in the method. A closer investigation of the solution to the linearized equations, however, indicated that the magnitude of this error depends strongly on the accuracy of the numerical approximation to the Fourier integral near $\omega = 0$, where $\bar{\tau} = 0$ and where $\partial\bar{\tau}/\partial\omega$ exhibits a singularity. This suggests a modification of the standard version of the spectral method such that a small correction term is added to the $\bar{\tau}$-distribution at $\omega = 0$ which accounts for the discretization error of the Fourier integral over the interval $-\frac{1}{2}\Delta\omega \leqslant \omega \leqslant \frac{1}{2}\Delta\omega$ and which is determined by the requirement that the numerical solution satisfies the asymptotic results for $x \to \infty$. Since the correction term influences the contribution of the interval centred at $\omega = 0$ to the Fourier integral, it gives rise to an additive constant in the wall-shear-stress distribution only. The problem of determining the magnitude of the correction term is therefore equivalent to the problem of calculating the point $x = x_n$ where $\tau(x, 0)$ changes its sign and where all field variables approximately assume their undisturbed values. The value of x_n was determined in two steps. First an estimate for x_n was obtained by calculating the distance x at which $\partial\tau(x, 0)/\partial x$ reached a minimum. Based on this estimate, the pressure distribution was evaluated by numerical integration over $\partial\tau/\partial z$ at $z = 0$ with $p(x_n) = 0$. Then, for large values of x, the pressure distribution was compared with the asymptotic result (36), and, if necessary, the calculation was repeated with a slightly changed value of x_n until the discrepancy reached a minimum. Finally, an estimate of the upstream decay rate k was determined from the numerical data. In all cases considered, this value differed from the exact solution to (20) by less than 1.5 %. For values of $a \geqslant 10$ the streamwise extent of the computational domain is not large enough even for small values of α for (34) to be applicable. In these cases, therefore, x_n had to be derived from the minimum of $\partial\tau(x, 0)/\partial x$ alone. Furthermore, it should be mentioned that the solution for large values of a represents the most severe test of the numerical method also for a different reason. While $\bar{\tau}(0; z) = 0$ for finite values of a, $\bar{\tau}$ itself exhibits a singularity at $\omega = 0$ for $a = \infty$. As a consequence, the standard version of the spectral method can no longer be used.

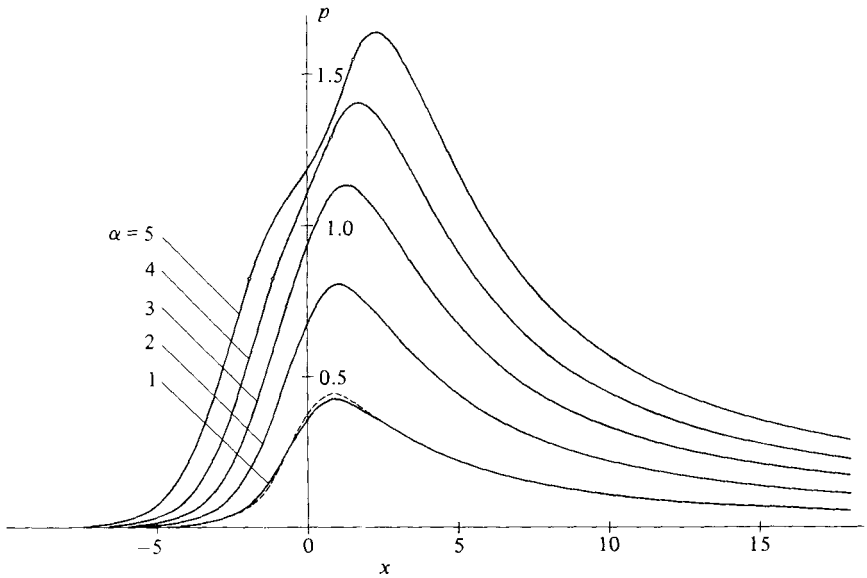

FIGURE 6. Cylinder–cone configuration given by (41): pressure distributions for $a = 1$ and various positive cone angles: -------, linear solution.

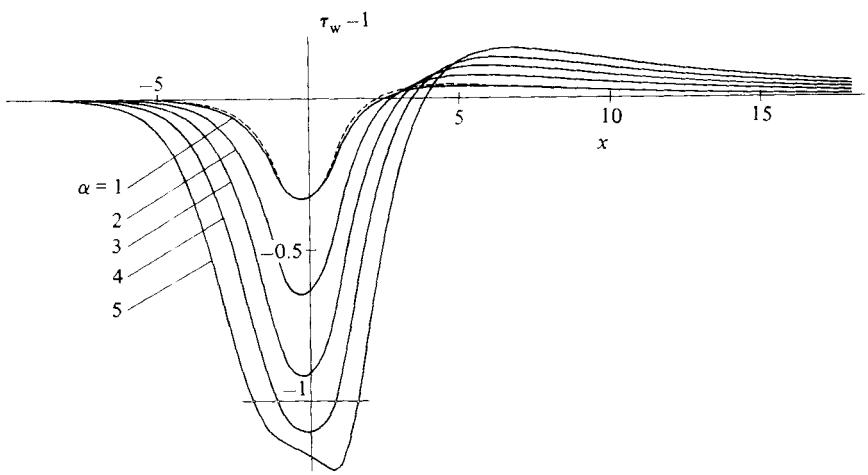

FIGURE 7. Cylinder–cone configuation given by (41): wall-shear-stress distributions for $a = 1$ and various positive cone angles: -------, linear solution.

To assess the accuracy of the method used here, the numerical results for $a = \infty$ were compared with the nonlinear solutions obtained by Rizzetta, Burggraf & Jenson (1978), who investigated planar supersonic flow over compression and expansion ramps. Although their computations were carried out for $\rho = 0$ (sharp corner), good agreement was observed for large values of α. In addition, a different finite-difference method using the implicit Crank–Nicolson scheme and a streamwise-marching procedure was developed which allowed one to calculate the field variables in the free-interaction region upstream of the cone for arbitrary values of a. Comparisons with the results obtained by means of the modified spectral method yielded complete agreement upstream of the separation point (figure 5).

Figures 6 and 7 show the influence of positive ramp angles α on the wall-shear-stress and pressure distributions for a fixed value of $a = 1$. Owing to the rounded corner, the minimum shear stress $\tau_{\min}$ occurs upstream of $x = 0$ if α is sufficiently small, in

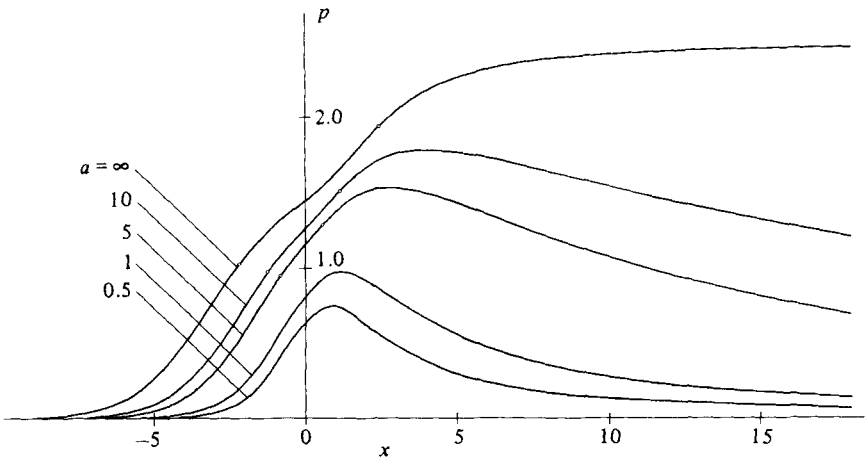

FIGURE 8. Cylinder–cone configuration given by (41): pressure distributions for $\alpha = 2.5$ and various values of a.

agreement with the linear solution, which has been included for comparison. As α increases, the wall shear stress decreases, the location of τ_{min} being almost unaffected as long as the flow remains attached. Once a separation bubble has formed for $\alpha > \alpha_{is} \approx 3.39$, however, the location of τ_{min} is shifted to larger values of x, and finally, for large values of α, the minimum wall shear stress occurs downstream of $x = 0$.

If the flow is unseparated, the pressure distributions for the various values of α are qualitatively similar to the linear result. For $\alpha > \alpha_{is}$, however, an inflection point develops within the separated region. A similar behaviour appears in two-dimensional flows, as shown by Rizzetta *et al.* (1978), where a plateau region of almost-constant pressure is formed for sufficiently large ramp angles. Unfortunately, no converged solutions could be obtained for $\alpha > 5$ using the spectral method. Free-interaction solutions with larger separated flow regions were obtained by means of a different finite-difference scheme mentioned earlier, and yielded even stronger evidence for the formation of a plateau region (e.g. figure 5, which suggests $\tau \to 0$ as $x \to \infty$). The analytical implications of these results are currently under investigation.

Finally, the value of the ramp angle $\alpha_{is} \approx 3.39$ at incipient separation obtained for the case $a = 1$, should be compared with the result $\alpha_{is} \approx 1.87$ for two-dimensional flows $a = \infty$. The strong influence of a on the pressure and shear-stress distributions can be seen also from figures 8 and 9, which summarize the effects of the body radius on the interaction process for a fixed cone angle $\alpha = 2.5$. In agreement with the trends exhibited by the linear solution presented in §4, the wall-shear-stress and pressure disturbances as well as the interaction length decrease with decreasing values of a, thus leading to larger values of α_{is}.

Results for negative cone angles $\alpha < 0$ are given in figures 10 and 11. As can be seen, the distributions of the wall shear stress and the pressure are qualitatively similar to the linear case for all values of α considered. However, while the location of the pressure minimum and the ratio $p_{min}/p(0)$ are virtually independent of α, the data for τ show that the point of maximum wall shear shifts downstream slowly as $|\alpha|$ increases. Furthermore, it is found that the minimum value of τ caused by the adverse pressure gradient downstream of the corner decreases progressively with α, indicating the possibility that the boundary layer separates downstream of the corner for sufficiently large values of $|\alpha|$ ($\alpha \lesssim -11.2$), in contrast with the two-dimensional counterpart of the flow. Clearly, further numerical and analytical efforts are necessary

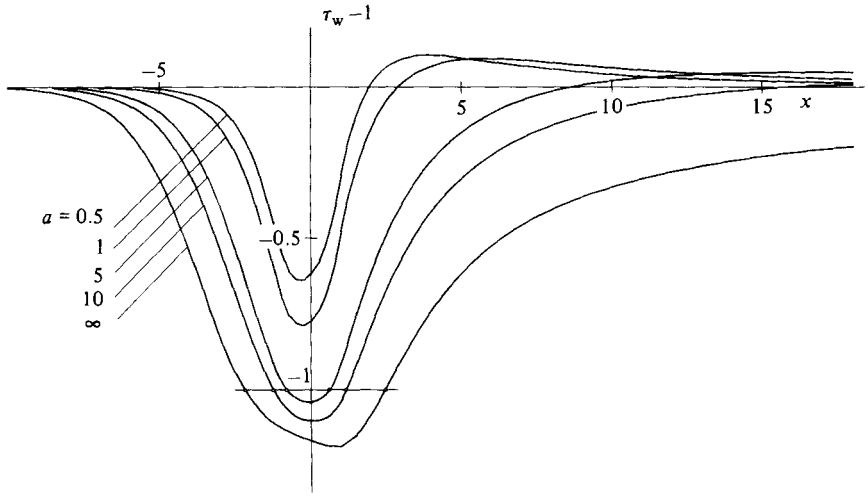

FIGURE 9. Cylinder–cone configuration given by (41): wall-shear-stress distributions for $\alpha = 2.5$ and various values of a.

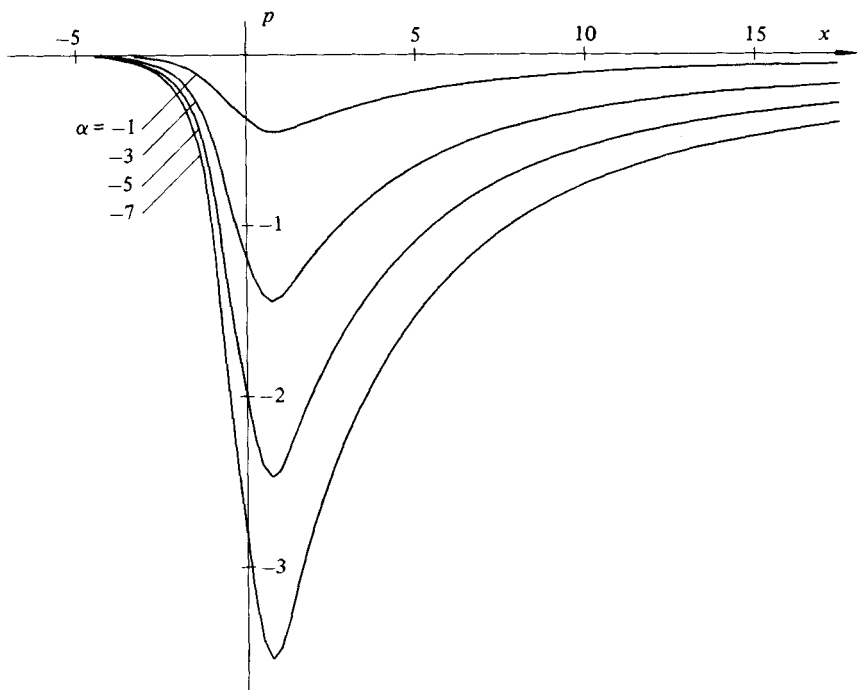

FIGURE 10. Cylinder–cone configuration given by (41): pressure distributions for $a = 1$ and various negative cone angles.

to elucidate the properties of axisymmetric flows over compression and expansion corners at large cone angles.

Figure 12 shows streamlines in the lower deck near the corner for $a = 1$ and $\alpha = 5$. As first derived by Oswatitsch (1958) using Taylor-series expansion of the full Navier–Stokes equations near $z = 0$, the angle θ between the wall and the separation or reattachment streamline is given by

$$\tan\theta = -3\left.\frac{\mathrm{d}\tau/\mathrm{d}x}{\mathrm{d}p/\mathrm{d}x}\right|_{z=0}. \tag{43}$$

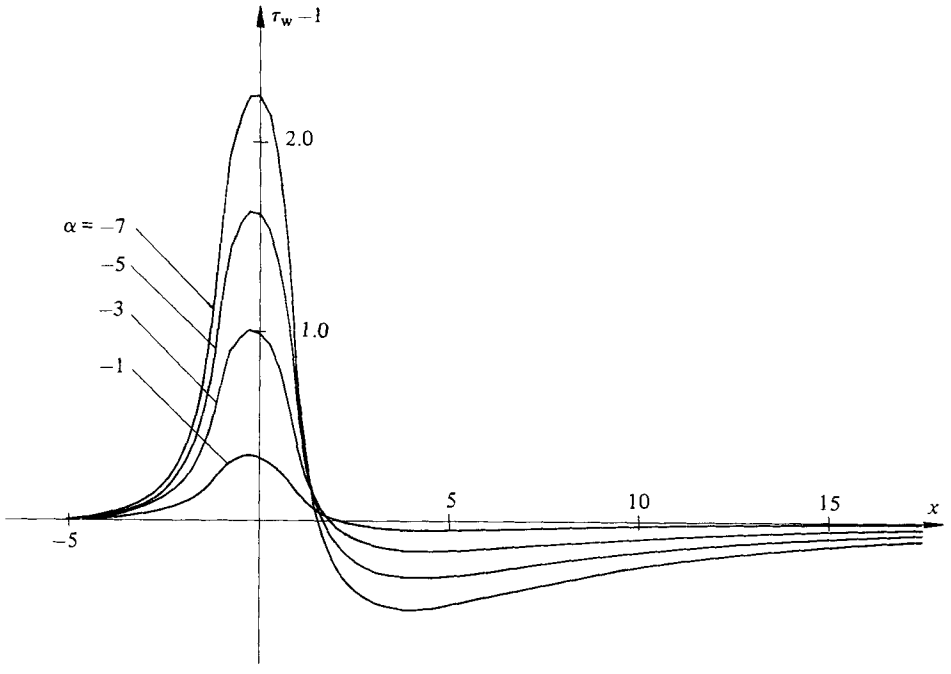

FIGURE 11. Cylinder–cone configuration given by (41): wall-shear-stress distributions for $a = 1$ and various negative cone angles.

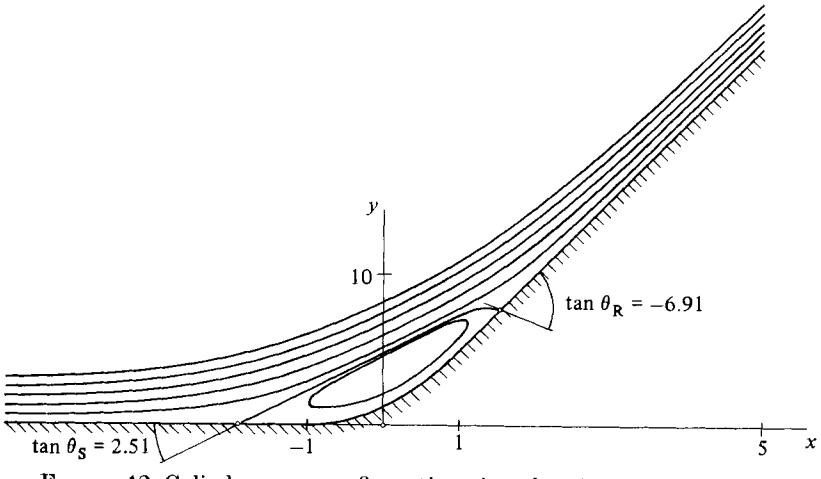

FIGURE 12. Cylinder–cone configuration given by (41): streamlines in the lower deck for $a = 1$, $\alpha = 5$.

This relationship can also be obtained directly from the lower-deck equations by Taylor-series expansions of u and v, which yield

$$\left.\begin{aligned} u &\sim \frac{\mathrm{d}\tau_w(x_0)}{\mathrm{d}x}(x-x_0)\,z+\frac{1}{2}\frac{\mathrm{d}P(x_0)}{\mathrm{d}x}z^2+\ldots, \\ v &\sim -\frac{1}{2}\frac{\mathrm{d}\tau_w(x_0)}{\mathrm{d}x}z^2+\ldots \end{aligned}\right\} \tag{44}$$

as the separation or reattachment point, $x = x_0$, $z = 0$, is approached, and it was found to be in complete agreement with our numerical results.

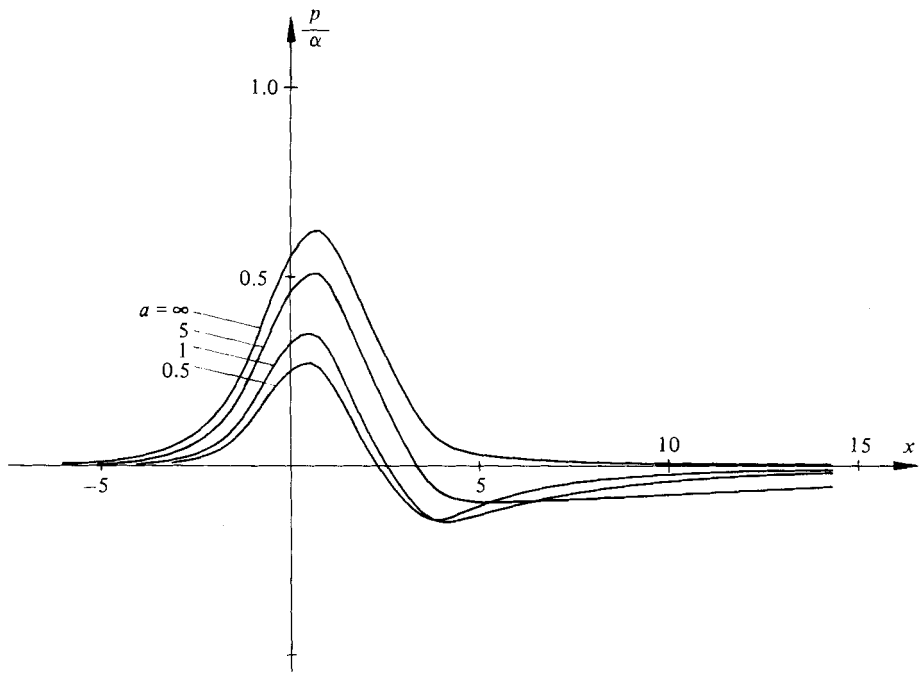

FIGURE 13. Pressure distributions for wall profiles given by (44) according to linear theory.

6. Smooth transition between two cylinders

As an example of an interaction process caused by a finite displacement of the incoming stream, the flow over two concentric cylinders of different radii which are connected by a smooth curve has been investigated. Specifically the profile chosen consisted of two parabolas extending from $x = -1$ to $x = 1$ and from $x = 1$ to $x = 4$ respectively (figure 14):

$$\left.\begin{aligned} F &= 0 \quad (x < -1), \\ F &= \tfrac{1}{4}\alpha(x+1)^2 \quad (-1 \leqslant x < 1), \\ F &= -\tfrac{1}{6}\alpha(1-8x+x^2) \quad (1 \leqslant x < 4), \\ F &= 2.5\alpha \quad (x \geqslant 4). \end{aligned}\right\} \tag{45}$$

Solutions to the linearized equations (27) and (28) are presented in figures 13 and 14. Owing to the smaller displacement effects caused by the wall shape (45) as compared with the rounded cylinder–cone combination, the disturbances of p and τ are substantially less in the free-interaction region $x \leqslant -1$. Furthermore, the pressure decays much faster to its unperturbed level, leading, however, in turn to a larger shear stress downstream of $x = 0$. The magnitude of the maximum shear-stress perturbation is influenced by two opposing trends. While the tendency to overshoot the unperturbed value $\tau = 1$ becomes more pronounced as a decreases (figures 4, 8) the growth rate of τ along the convex portion of the wall is larger for large values of a. Consequently, the maximum of the wall-shear-stress distribution is largest at intermediate values of $a \approx 5$.

Nonlinear solutions have been also calculated for several values of a when $\alpha = 4$. These results are summarized in figures 15 and 16.

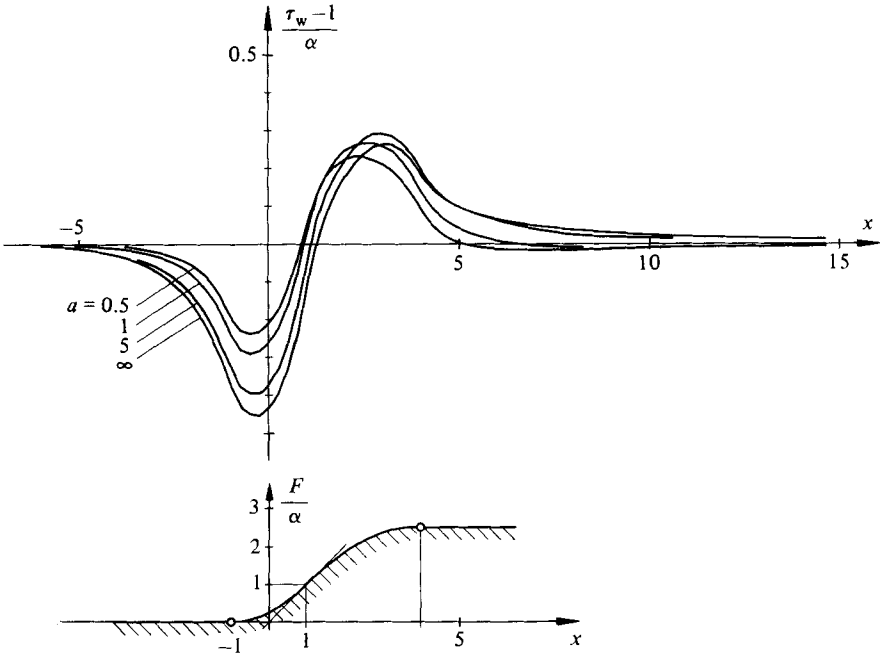

FIGURE 14. Wall-shear-stress distributions for wall profiles given by (44) according to linear theory.

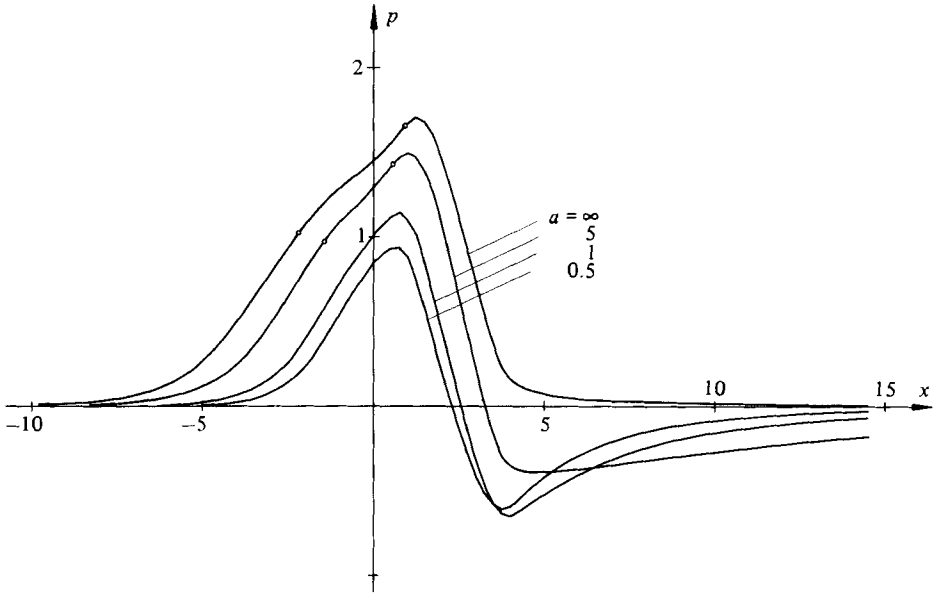

FIGURE 15. Pressure distributions for bodies given by (44): nonlinear solutions for $\alpha = 4$ and various values of a.

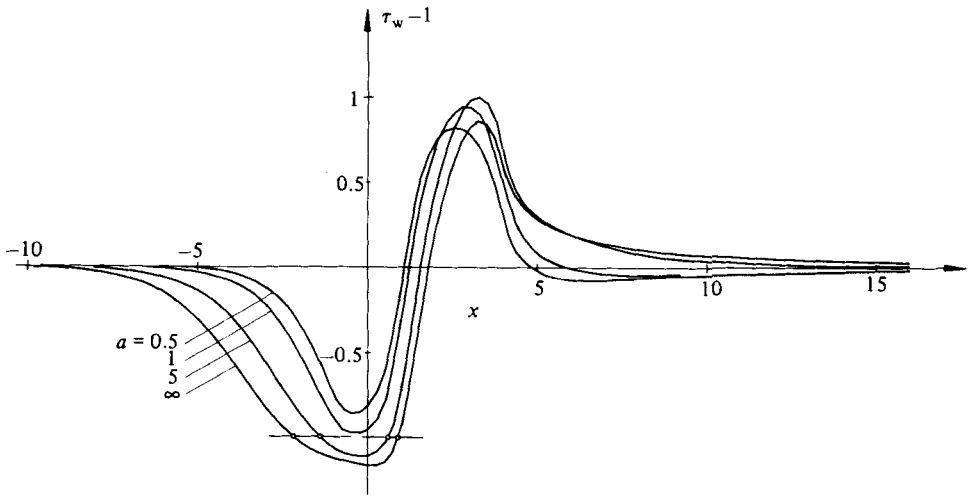

FIGURE 16. Wall-shear-stress distributions for bodies given by (44): nonlinear solutions for $\alpha = 4$ and various values of a.

7. Concluding remarks

Viscous–inviscid interactions on axisymmetric bodies flying at supersonic speeds have been investigated under the assumption that the Reynolds number is large and that the characteristic body radius is of the same order of magnitude as the length of the interaction region. As a consequence, the governing equations for the flow inside the boundary layer are of the same form as in the two-dimensional case to leading order, while the axisymmetry of the flow makes itself felt through the relationship between the induced pressure and the displacement thickness.

Detailed numerical and analytical studies have been carried out for bodies of revolution of the cylinder–cone type and have revealed several differences from the corresponding two-dimensional interaction problem. It was found that the upstream interaction region is shorter than that in the two-dimensional case. Also, it has been shown that the pressure disturbance decays to zero far downstream, in contrast with the two-dimensional case, where the pressure approaches a non-zero constant value. In addition, the numerical computations show that the incipient separation angle for compressive interactions is significantly higher for the flared cone than for the ramp problem.

In the numerical and analytical studies presented here it has also been shown that the interaction region decreases in size as the body radius a decreases, and in fact vanishes in the limit as $a \to 0$ in the current scaling. This result implies that a new structure for the interaction region will emerge when the body thickness becomes of the same order as the boundary-layer thickness, as discussed by Duck (1984) in his study of incompressible flows.

Finally it is noted that the linearized solutions presented here differ significantly from these presented by Huang & Inger (1983) owing to a mathematical error present in their formulation.

One of the authors (A. Kluwick) gratefully acknowledges the hospitality of the Department of Engineering Science and Mechanics at Virginia Polytechnic Institute and State University during the preparation of this work.

REFERENCES

BRILLIANT, H. M. & ADAMSON, T. C. 1973 Shock-wave–boundary-layer interactions in laminar transonic flow. *AIAA Paper* 73–239.

BURGGRAF, O. R. & DUCK, P. 1981 Spectral computation of triple deck flows. In *Proc. 1st Symp. on Physical and Numerical Aspects of Aerodynamic Flows, California State University, Long Beach.*

COOLEY, J. W. & TUKEY, J. W. 1965 *Math. Comp.* **19**, 297.

DUCK, P. 1984 The effect of a surface discontinuity on an axisymmetric boundary layer. *Q. J. Mech. Appl. Maths* (in press).

GITTLER, P. 1984 Laminare Wechselwirkungsvorgaenge am schiebenden Fluegel bei Ueberschallstroemung. *Z. angew. Math. Mech.* **64**, T108 (in press).

HUANG, M. & INGER, G. R. 1983 Application of the triple-deck theory of viscous–inviscid interactions to bodies of revolution. *J. Fluid Mech.* **129**, 427.

KLUWICK, A. 1979 Stationaere, laminare wechselwirkende Reibungsschichten. *Z. Flugwiss. Weltraumf.* **3**, 157.

LIGHTHILL, M. J. 1945 Supersonic flow past bodies of revolution. *ARC R&M* 2003.

LIGHTHILL, M. J. 1953 On boundary layers and upstream influence II. Supersonic flow without separation. *Proc. R. Soc. Lond.* A **217**, 478.

LIGHTHILL, M. J. 1958 *An Introduction to Fourier Analysis and Generalized Functions.* Cambridge University Press.

MESSITER, A. F. 1970 Boundary layer flow near the trailing edge of a flat plate. *SIAM J. Appl. Maths* **18**, 241.

MESSITER, A. F. 1978 Boundary layer separation. In *Proc. 8th US Natl Congr. Appl. Mech.*, p. 157.

MESSITER, A. F. 1983 Boundary layer interaction theory. *Trans. ASME* E: *J. Appl. Mech.* (to appear).

OSWATITSCH, K. 1958 Die Abloesebedingung von Grenzschichten. In *Grenzschichtforschung* (ed. H. Goertler), p. 357. Springer.

RIZZETTA, D., BURGGRAF, O. & JENSON, R. 1978 Triple-deck solutions for viscous supersonic and hypersonic flows past corners. *J. Fluid Mech.* **89**, 535.

ROSENHEAD, L. 1963 *Laminar Boundary Layers.* Oxford University Press.

SMITH, F. T. 1976 Pipeflows distorted by nonsymmetric indentation or branching. *Mathematika* **23**, 62.

SMITH, F. T. 1982 On the high Reynolds number theory of laminar flows. *IMA J. Appl. Maths* **28**, 207.

SMITH, F. T., SYKES, R. I. & BRIGHTON, P. W. M. 1977 A two-dimensional boundary layer encountering a three-dimensional hump. *J. Fluid Mech.* **83**, 163.

STEWARTSON, K. 1955 The asymptotic boundary layer on a circular cylinder in axial incompressible flow. *Q. Appl. Maths* **13**, 113.

STEWARTSON, K. 1969 On the flow near the trailing edge of a flat plate II. *Mathematika* **16**, 106.

STEWARTSON, K. 1970*a* On supersonic boundary layers near convex corners. *Proc. R. Soc. Lond.* A **319**, 289.

STEWARTSON, K. 1970*b* On laminar boundary layers near corners. *Q. J. Mech. Appl. Maths* **23**, 137.

STEWARTSON, K. 1971 On laminar boundary layers near corners: corrections and an addition. *Q. J. Mech. Appl. Maths* **24**, 387.

STEWARTSON, K. 1974 Multistructured boundary layers on flat plates and related bodies. *Adv. Applied Mech.* **14**, 145.

STEWARTSON, K. 1980 High Reynolds number flows. In *Approximation Methods for Navier–Stokes Problems* (ed. R. Rautmann), p. 505. Springer.

STEWARTSON, K. 1981 D'Alembert's Paradox. *SIAM Rev.* **23**, 308.

STEWARTSON, K. & WILLIAMS, P. G. 1969 Self-induced separation. *Proc. R. Soc. Lond.* A **312**, 181.

SYKES, R. I. 1980 On three-dimensional boundary layer flow over surface irregularities. *Proc. R. Soc. Lond.* A **373**, 311.

VATSA, V. N. & WERLE, M. J. 1977 Quasi-three-dimensional laminar boundary-layer separations in supersonic flow. *Trans. ASME* I: *J. Fluids Engng* **99**, 634.

WARD, G. N. 1948 The approximate external and internal flow past a quasi-cylindrical tube moving at supersonic speeds. *Q. J. Mech. Appl. Maths* **1**, 225.

WARD, G. N. 1955 *Linearized Theory of Steady High Speed Flow*. Cambridge University Press.